Nano Energy 31 (2017) 351–358

Contents lists available at ScienceDirect

Nano Energy

journal homepage: www.elsevier.com/locate/nanoen

Integrated triboelectric nanogenerator array based on air-driven membrane structures for water wave energy harvesting

Liang Xu[a], Yaokun Pang[a], Chi Zhang[a], Tao Jiang[a], Xiangyu Chen[a], Jianjun Luo[a], Wei Tang[a], Xia Cao[a,c,*], Zhong Lin Wang[a,b,*]

[a] Beijing Institute of Nanoenergy and Nanosystems, Chinese Academy of Sciences; National Center for Nanoscience and Technology (NCNST), Beijing 100083, PR China
[b] School of Material Science and Engineering, Georgia Institute of Technology, Atlanta, GA 30332, USA
[c] School of Chemistry and Biological Engineering, University of Science and Technology Beijing, Beijing 100083, PR China

ARTICLE INFO

Keywords:
Triboelectric nanogenerator array
Water wave energy
Air-driven mechanism
Membrane-based structure
Blue energy

ABSTRACT

Water wave energy is considered a promising renewable energy source, while currently little has been exploited due to a number of unsolved challenges for present technologies. The triboelectric nanogenerator (TENG), as an emerging energy harvesting technology, shows particular advantages in transforming low frequency mechanical energy into electricity, providing new opportunities for harvesting water wave energy. In this work, an integrated triboelectric nanogenerator array device based on air-driven membrane structures is demonstrated. With novel designs of a spring-levitated oscillator structure and a mechanism to use air pressure to transfer and distribute harvested water wave energy, the device can drive a series of integrated TENG units effectively and simultaneously. While operating at low frequency near the resonant frequency of about 2.9 Hz, the device integrating 38 TENG units shows high output of transferred charges per cycle of 15 μC, short-circuit current of 187 μA and optimized peak power density of 13.23 W m^{-3}. The device can easily integrates large-scale high-density TENG arrays in one package, as can greatly augment the output, providing a promising route to effectively harvest water wave energy for various practical applications.

1. Introduction

Renewable and clean energy has been endowed increasingly significance all over the world, owing to the ever greater environmental problems and resource exhausting for exploiting traditional fossil fuels [1–4]. The ocean contains abundant energy, both renewable and clean, in the form of wave energy, tidal energy, current energy, thermal energy and osmotic energy [5–7]. At present, an electromagnetic generator with various mechanical structures is the major technological scheme for extracting ocean energy [7–10]. Although being developed for decades, it is still facing great engineering difficulties, not easy to scale-up, and suffering from high cost, resulting in a low exploiting level [7–9]. Among various alternative energy scavenging technologies, such as approaches by photovoltaic [11,12], piezoelectric [13–16], and thermoelectric [17,18] effects, the triboelectric nanogenerator (TENG), based on the conjunction of contact electrification and electrostatic induction, shows merits of low cost, light weight, simple structure and abundant choice of materials [19–23]. It has particular advantages in transforming low frequency mechanical energy into electricity [24], and the efficiency and output power has been greatly elevated in recent few years [25–30], providing new opportunities for large-scale harvesting of water wave energy in the ocean and other water bodies [31–35]. Previous works have demonstrated the possibility of using TENGs in water wave energy harvesting, mainly employing ball-shell structures [34–38]. Such structures typically have only one TENG unit in working at one time in a single package. Though can be organized in groups using several devices [35], it should be more efficient and compact while simultaneously driving several TENG units in a single packaged device.

Here, an integrated triboelectric nanogenerator array device based on air-driven membrane structures is presented. With novel designs of a spring-levitated oscillator structure and a mechanism to use air pressure to transfer and distribute harvested water wave energy, a high-density array of TENG units integrated in the device can be driven simultaneously and effectively. A device packaging 38 single TENG units is demonstrated. While operating at low frequency near the resonant frequency of about 2.9 Hz, the device shows high output of transferred charges per cycle of 15 μC, short-circuit current of 187 μA

* Corresponding authors at: Beijing Institute of Nanoenergy and Nanosystems, Chinese Academy of Sciences; National Center for Nanoscience and Technology (NCNST), Beijing 100083, PR China.
E-mail addresses: caoxia@binn.cas.cn (X. Cao), zlwang@binn.cas.cn (Z.L. Wang).

http://dx.doi.org/10.1016/j.nanoen.2016.11.037
Received 19 September 2016; Received in revised form 14 November 2016; Accepted 17 November 2016
Available online 24 November 2016

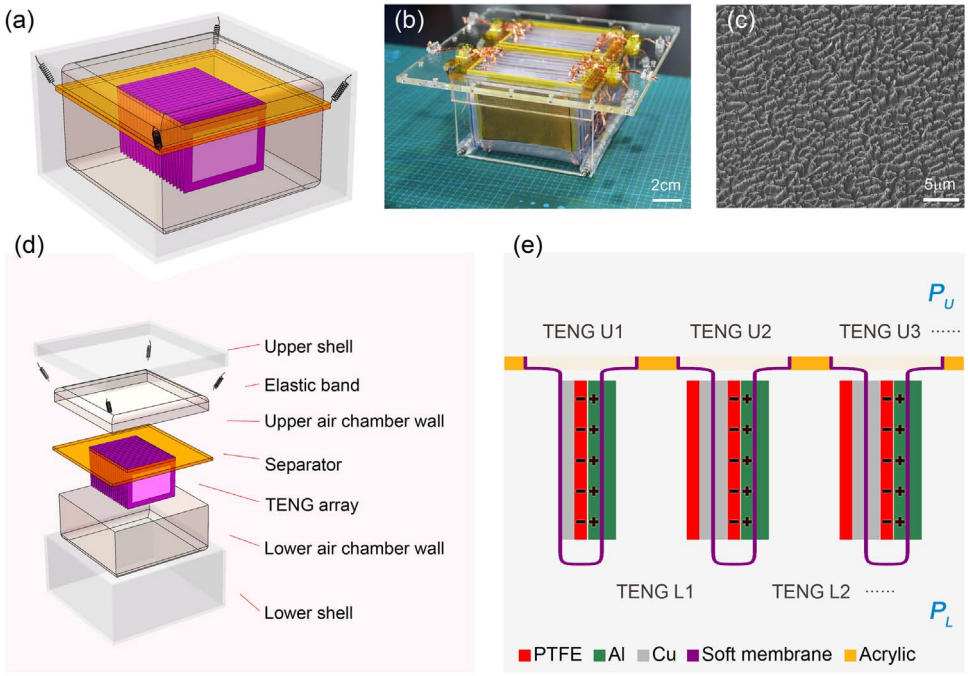

Fig. 1. Structure of the TENG array device. (a, d) Schematic diagrams of the structural design of the device, and (d) shows an exploded view of the device structure. (b) Photograph of the fabricated TENG array and the separator. (c) SEM image of nanostructures on the PTFE surface. (e) Sectional view and detailed structure of the TENG array. P_U and P_L represent the pressure in the upper and lower air chambers, respectively.

and optimized peak power density of 13.23 W m^{-3}. The output would increase with augmented size of the array, providing a promising route to efficiently harvesting water wave energy for various practical applications.

2. Results and discussion

The basic structure of the device is shown in Fig. 1a. It is mainly composed of two parts, the inner oscillator and the outer shell. The oscillator is connected to the shell with elastic bands, forming a spring-levitated oscillator structure. Fig. 1d gives an exploded view of the device. The shell is composed of the upper shell and the lower shell, both made of acrylic. The oscillator can be further divided into several parts, as the upper and the lower air chamber wall made of soft membrane, the separator made of acrylic, the TENG array. The soft membrane contains 20% nylon and 80% polyethylene, and can endure high pressure up to 80 KPa. The function of the shell is as a mounting base and an enclosed protector to the oscillator, and the oscillator

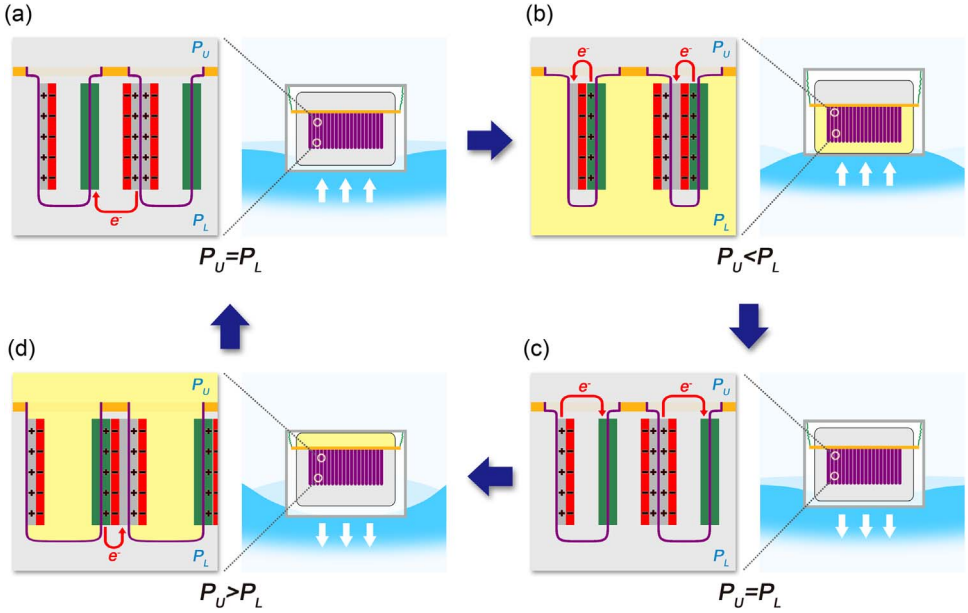

Fig. 2. Working principle of the TENG array device. (a) The outer shell moves upwards with the water wave (shown in the right). There is $P_U = P_L$, and the upper and lower TENG units are all in separate state (shown in the left). (b) The shell moves upwards further and the bottom of the lower chamber is pressed by the shell, causing $P_U < P_L$. The pressure difference drives the reshape of the soft membranes and makes the upper units into contact state and the lower ones into fully separate state. (c) The outer shell moves downwards. There is $P_U = P_L$, and the upper and lower TENG units get into separate state. (d) The shell moves downwards further and the top of the upper air chamber is pressed by the shell, causing $P_U > P_L$. The upper units get into fully separate state and the lower units into contact state. For simplicity, the movement of the inner oscillator corresponding to the water waves is neglected in above descriptions, and the external circuit for charge transfer are not shown in the figures.

collects mechanical energy, then translate it into electricity. The structure is quite stable due to that the elastic bands can provide elastic force both in horizontal and perpendicular direction to the mass center of the oscillator and make the oscillator seated firmly in position in the shell.

Fig. 1e illustrates the detailed structure of the TENG array and the separator with a sectional drawing. Soft membranes are glued to a hole in the center of the separator to form air-pocket-like structures, and separate the air chamber into the upper one and the lower one with pressures denoted as P_U and P_L respectively, which would reshape the soft membranes while the pressure changes. Rectangular TENG electrodes are attached to soft membranes to form TENG units in the way as shown in the sectional drawing, thus can move when soft membranes deform. There are two kinds of TENG units, denoted as TENG U*n* and TENG L*n* (n=1,2,...), based on whether their electrodes are attached to the upper side or lower side of the soft membranes, and they form a TENG array which can be divided further as the upper TENG array and the lower one. The two electrodes in a single TENG unit are a Cu foil covered by a 50 μm thick polytetrafluoroethylene (PTFE) film, and a Al foil, respectively, with a dimension of 4.5 cm×7.5 cm. The maximum distance of the two electrodes, namely the gap size, is set to 6 mm, which is reasonable to get both high transferred charges and open-circuit voltage, as shown in Fig. S1. Nanostructures are fabricated on PTFE surfaces to enhance the contact electrification effect, which is important to elevate the output of TENGs (Fig. 1c) [39–41]. The photograph of a constructed TENG array and separator is presented in Fig. 1b.

The fundamental working principle of the TENG units is based on the conjunction of contact electrification and electrostatic induction [20]. When the pressure drives the TENG units into contact state (Fig. 1e), there would generate positive charges on the Al surface and negative ones on the PTFE surface due to contact electrification effect. Afterwards, when the two surfaces are separated by an external force, a potential drop is created, which drives the free electrons in Cu foil to move to the Al foil through an external circuit to achieve a balanced state, showing an electrostatic induction effect. When the TENG units get into contact state again, electrons would move back to Cu foil to maintain the balanced state.

A detailed cycle with four stages for the working process of the device is shown in Fig. 2, without illustrating the above initial contact electrification process. When the water wave pushes the outer shell to move upwards (Fig. 2a–b), the inner oscillator goes down relative to the shell, thus compresses the lower air chamber, inducing $P_U < P_L$. The pressure difference P_{Diff} reshapes the soft membranes and makes the upper TENG units into contact state and the lower TENG units into fully separate state. Electrons would move from Al foils to Cu foils in the upper TENG units and from Cu foils to Al foils in the lower TENG units, generating current in the external circuit. When the shell moves downwards with the water wave (Fig. 2c to d), the inner oscillator goes up relative to the shell, thus compresses the upper air chamber, causing $P_U > P_L$. The pressure difference reshapes the soft membranes and makes the upper TENG units into fully separate state and the lower TENG units into contact state, accompanied by electrons moving from Cu foils to Al foils in the upper TENG units and from Al foils to Cu foils in the lower TENG units through the external circuit. In such a way, the device can generate electricity corresponding to the water wave. The structures and the parameters are elaborately adjusted to make sure the device would function with tiny stimulations.

The electrical output characteristics of a single TENG unit are measured and shown in Fig. 3. The open-circuit voltage of a single unit

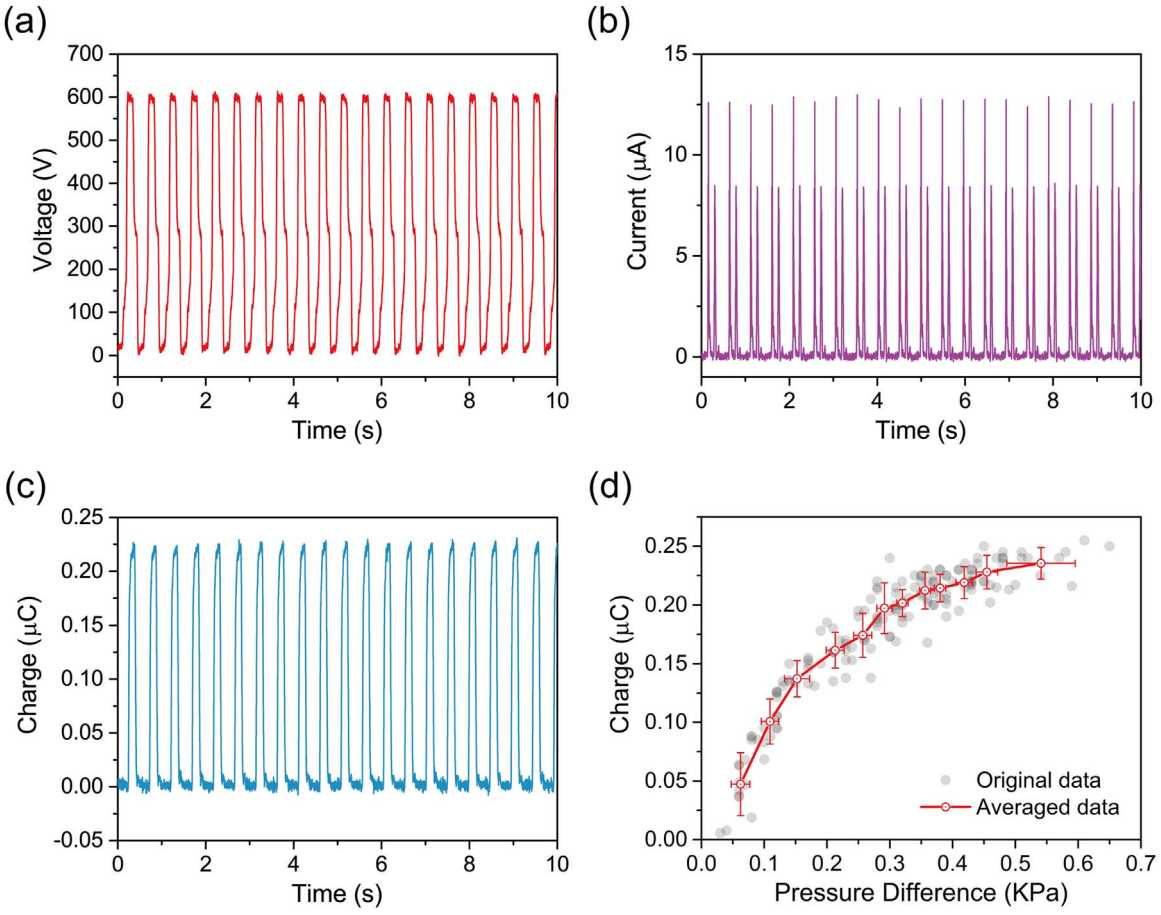

Fig. 3. Electrical output characterization of a single TENG unit. (a–c) Open-circuit voltage, rectified short-circuit current, and transferred charge of the single TENG unit. (d) Dependence of the transferred charges on the pressure difference between the upper and lower air chambers.

V_{OCS} reaches 600 V (Fig. 3a). The peak rectified short-circuit current I_{SCS} is 12.5 μA, and the transferred charge Q_{SCS} is 0.22 μC per cycle, as shown in Fig. 3b and c respectively. The pressure difference P_{Diff} between the two air chambers is crucial to the output of TENG units. Fig. 3d shows the relationship between the transferred charges and the peak driving pressure difference. With the increase of pressure difference from 0 to 0.35 kPa, the amount of transferred charges increases rapidly to about 0.21 μC. Afterwards, the transferred charges would still grow with rising pressure difference, yet with gradually slower rate. This indicates that with relatively small pressure, the two electrodes of single TENG units can get into a good contact state, which affects the transferred charges. The deviation in the figure should be attributed to the complex factors that affect the transferred charges under the same pressure difference, like the surface contact condition, the reshape of the soft membranes and the air flow etc. The durability of TENG units is also tested, with several thousand cycles, as shown in Fig. S2. The output short-circuit current only has small variations during the test, as can be attributed to the uncertainty in the pressure-charge relation, indicating good durability in long-time operation.

A device containing 38 TENG units is fabricated, that is made of 20 TENG units in the upper array and 18 TENG units in the lower array. The TENG units in the upper array or the lower array are parallel connected respectively, namely all the PTFE+Cu electrodes in one array are electrically connected and so do the Al electrodes. Due to the output phase of the upper array and the lower array are not consistent, the outputs of the two arrays would first get through respective rectifiers, then connect together to produce the entire output of the device, as shown in Fig. 4d. A vibration generator is used to push the bottom of the shell of the device in the vertical direction, to simulate the driving effect of water waves (Fig. S3). The vibration generator typically inputs a sinusoidal motion to the shell, with 3.4 Hz frequency and 8 mm amplitude. The frequency is near the resonant frequency of the device as will be discussed later. The amplitude is subjected to the motion capability of the vibration generator.

Fig. 4 shows the outputs of the device driving by the vibration generator. Without a rectifier, the open-circuit voltage of the upper array V_{OCU} is 610 V (Fig. 4a). The peak short-circuit current I_{SCU} is 126 μA (Fig. 4b). The transferred charge Q_{SCU} is 4.5 μC per cycle (Fig. 4c). Due to the feature of parallel connection, the open-circuit voltage of the upper array is comparable to that of a single TENG unit, and the amount of transferred charges is roughly the superposition of that of 20 single TENG units. The short-circuit current is decided by the change rate of the transferred charge $I_{SCU} = dQ_{SCU}/dt$[42]. The outputs of the lower array have similar characteristics as the upper array. Considering the whole device using rectifiers, the peak short-circuit current I_{SC} reaches 187 μA, and the short-circuit accumulative

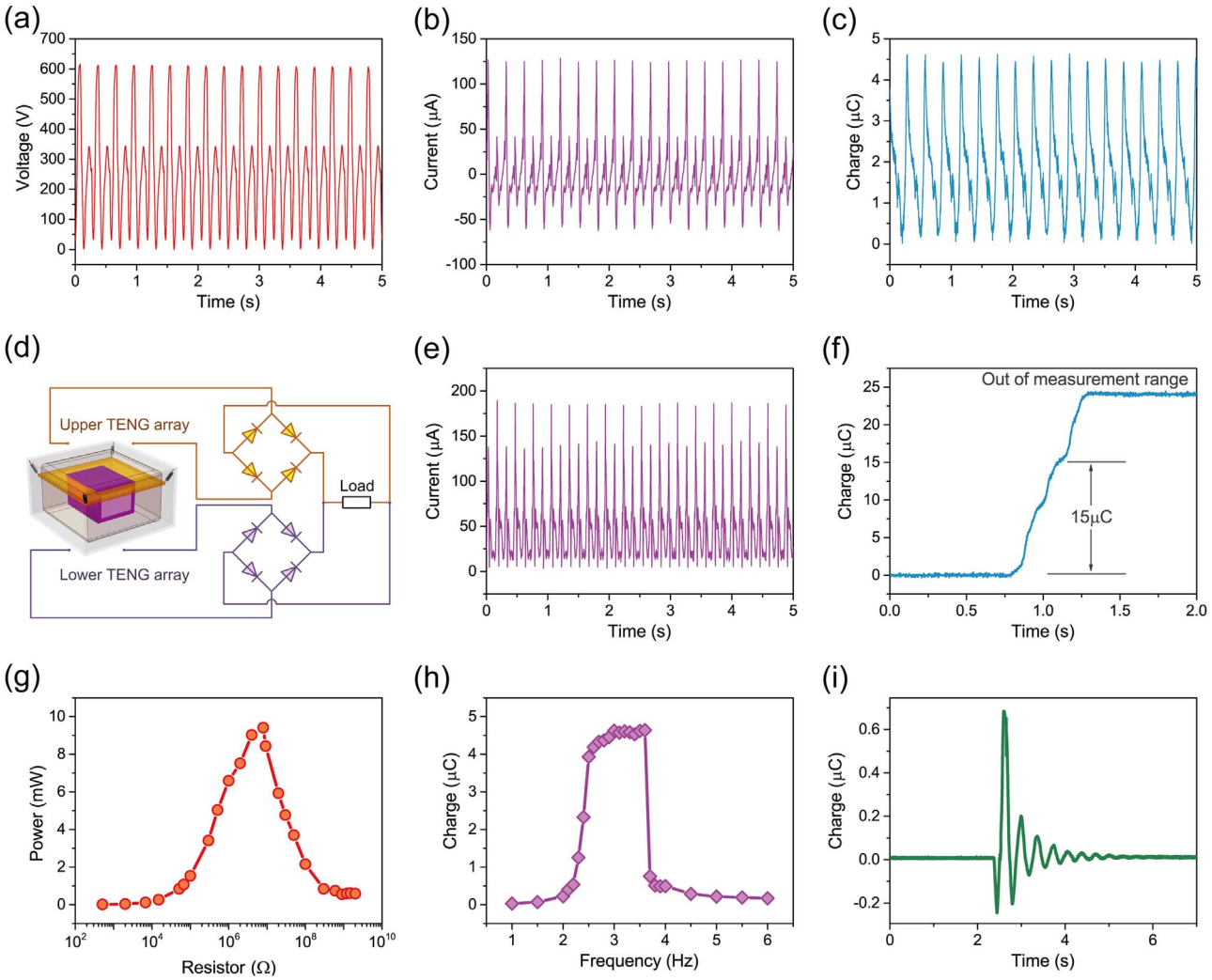

Fig. 4. Electrical output and dynamic characteristics of the TENG array device. (a–c) Open-circuit voltage, short-circuit current, and transferred charge of the upper TENG array. The electrometer has a charge measurement range up to about 25 μC. (d) Schematic diagram of the rectification circuit for the whole device. (e, f) Rectified short-circuit current and transferred charge of the whole device. (g) Dependence of the output peak power of the device on a resistive load. (h) Dependence of the transferred charges of the upper TENG array on the driving frequency. (i) Oscillatory output of the upper TENG array under a single impact on the bottom of the outer shell.

charge Q_{SC} is 15 μC per cycle, as shown in Fig. 4e and f. To test the output power of the device, different resistors are connected to the circuit as a load. The relationship of the peak power P to resistor R is shown in Fig. 4g. It is evident that there exists an optimal resistive load, about 8 MΩ, when the power reaches the largest value of about 10 mW, consistent with previous theoretical results [42,43]. Considering the volume of the TENG array, the optimized peak power density is 13.23 W m^{-3}.

The frequency characteristic of the device is crucial to its performance. When the frequency of the inner oscillator is equal to the frequency of the driver, e.g. water waves, the device would enter a resonant state, and the energy harvesting efficiency would be the highest. The frequency of the oscillator can be estimated theoretically. In the fabrication of the device, the oscillator is designed to let its gravity force equal to the elastic force of the elastic bands, thus the oscillator is actually like levitating in the shell, referring to the spring-levitated oscillator structure. This design ensures that the oscillator would vibrate under tiny water waves. In such context, $kl = mg$, where k is the stiffness of the elastic bands, l is the static stretch length, and m is the mass of the oscillator. Meanwhile, the vibration frequency of a spring-oscillator system would be:

$$f = \frac{1}{2\pi}\sqrt{\frac{k}{m}} \tag{1}$$

By simple substitution, one can get:

$$f = \frac{1}{2\pi}\sqrt{\frac{g}{l}} \approx \frac{0.5}{\sqrt{l}} \tag{2}$$

While not considering complex factors like damping and dissipation, Eq. (2) gives a good semi-quantitative and convenient estimation to the resonant frequency of the device. Here, the device has an equivalent static stretch length of 3 cm considering the nonlinearity. According to Eq. (2), its theoretical vibration frequency is about 2.9 Hz. This is consistent with the experiment results as shown in Fig. 4h. When the vibration generator drives the shell with sinusoidal motion of different frequency and same amplitude 8 mm, the inner oscillator would oscillate in different amplitude, thus would affect the output of the TENG array. Take the transferred charge of the upper TENG array as an indicator. In the frequency range of 2.5–3.6 Hz, there would be an output plateau about 4.5 μC, showing a near resonant state. Beyond the above frequency range, the output decreases rapidly. However, this does not mean that the device can only work in such a frequency range. With driving amplitude much larger than 8 mm, greater oscillation would be stimulated, though not in a resonant way, resulting in the enhancement of the output. Moreover, according to Eq. (2), such frequency can be tuned by simply adjusting the static stretch length l, depending on the characteristics of specific water circumstance where the device would work in. The device also has the ability to output several cycles under one impact. Fig. 4i shows the transferred charges of the upper array under a 8 mm pulse drive at the bottom of the shell. The output continues after the pulse, and gradually decays to zero after about 10 cycles. It implies that the device has the ability to absorb mechanical energy in single pulses and store it in the form of oscillation energy, which gradually converts into electricity afterwards. This is significant to improve the output of the device working in real circumstance considering the randomicity of the motion of water waves.

To better understand how the air chambers drive the TENG array, a theoretical model is established. While in operation, the air-pocket-like structures of the TENG array would expand or contract, accompanying the up and down movement of the top of the upper chamber or the bottom of the lower chamber, which is driven by contacts with the outer shell. Due to the relative low pressure, the air compression in the air chambers can be neglected and their volume is constant. Based on

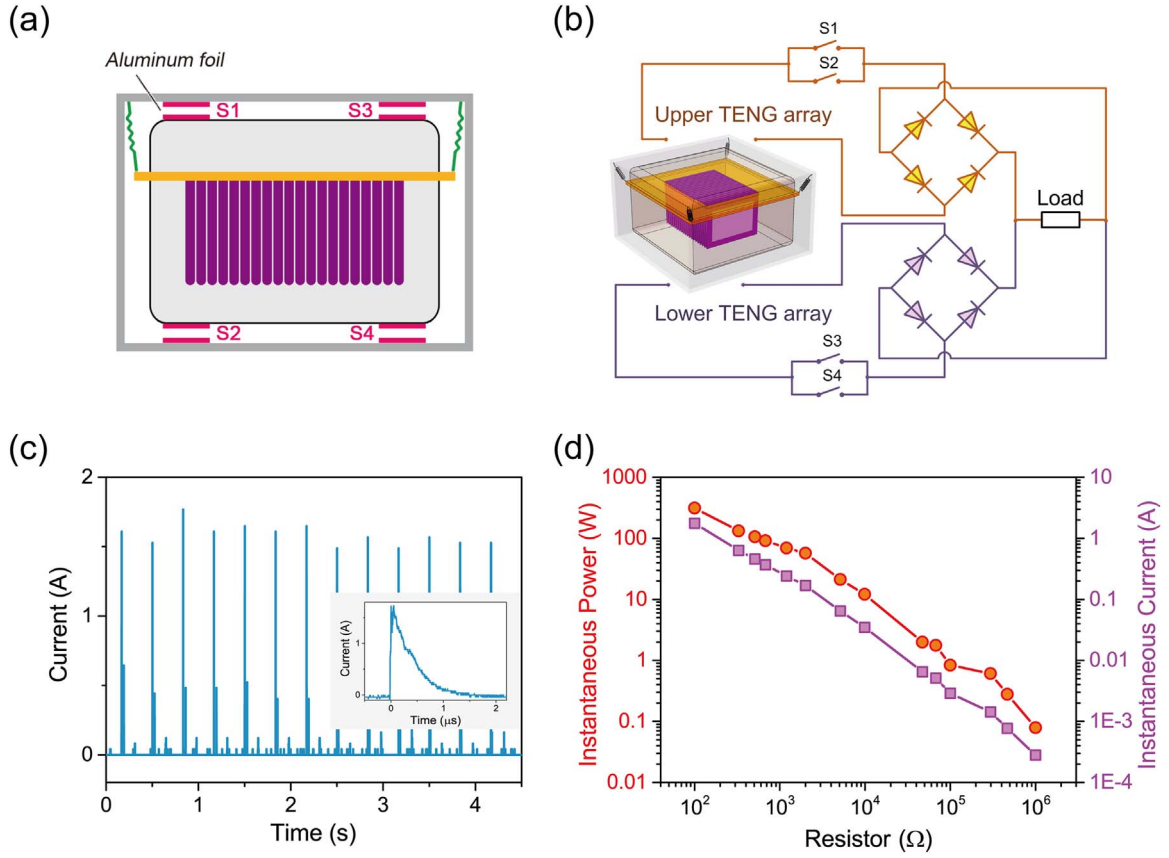

Fig. 5. The TENG array device with a switch circuit. (a) Schematic illustration of the structure of switches. (b) Schematic diagram of the switch circuit. (c) Pulse current of the device. Inlet: single current pulse. (d) Dependence of the pulse current and the instantaneous output power on a resistive load.

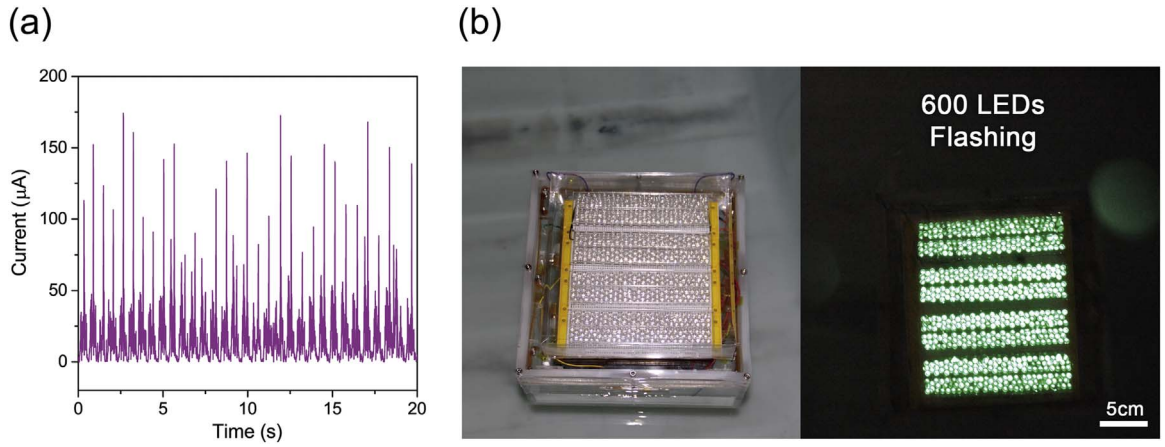

Fig. 6. The TENG array device working on water. (a) Short-circuit current without a switch circuit. (b) Photographs of the device with 600 LEDs floating on water before and after being lighten up.

such constant volume relation, there is:

$$S_{AC}x = NS_{TENG}d \tag{3}$$

where S_{AC} is the area of the top of the upper air chamber or the bottom of the lower chamber, x is the length that the top or the bottom moves, N is the number of air-pocket-like structures in the array, S_{TENG} is the area of one sidewall of air pockets that TENG electrodes are attached to, d is the relative movement of a pair of TENG electrodes in normal direction. The pressure in each air chamber can be regarded as equal anywhere, and for the chamber in low pressure state, the pressure is usually equal to the pressure of circumstance owing to the slack chamber wall in such a state. For the air chamber in high pressure state, the pressure transfers the force from the top or the bottom of the air chamber to the TENG electrodes:

$$\frac{F_{AC}}{S_{AC}} = \frac{F_{TENG}}{S_{TENG}} \tag{4}$$

where F_{AC} is the pressure force on the top or bottom of the air chamber originating from the contact with the outer shell, F_{TENG} is the force on the sidewall of air pockets that TENG electrodes are attached to. Eqs. (3) and (4) indicate that with air pressure as a medium, the force and movement from the outer shell is transferred and distributed into each air pocket, then drives each TENG unit. This is also how the mechanical energy flows. Owing to the flexibility of the membranes and the pressure equality in air chamber space, all the TENG units should be able to achieve good contact state which is vital to the output, no matter how many units there exist. The above mechanism ensures that all the TENG units in one device can be driven effectively and simultaneously, unlike previous works where only one TENG unit in a device is driven at one time [34,35]. This also implies that the TENG array has superior ability for extension, and there can integrate massive TENG units in only one package, achieving much higher output.

The power output of the device can be further improved by a switch circuit for high pulse power applications, as shown in Fig. 5a and b. Al foils are attached to the top or the bottom of the air chambers, and to the corresponding positions of the outer shell, forming four contact switches S1, S2, S3, S4, as shown in Fig. 5a. The switches are closed while corresponding foils contact. Thus when the inner oscillator moves to the highest position, S1 and S3 would be closed, and when the inner oscillator moves to the lowest position, S2 and S4 would be closed. This four switches are connected into the circuit as in Fig. 5b. With the switches, the device would only have output when the inner oscillator is near the highest or lowest position, before which voltage has been established between Cu and Al foils due to charge separation. Once the switches are closed, free charges would flow through the external circuit by the drive of the voltage. Such a switch circuit greatly reduces the duration of the charge transfer process, intensifying the output current and power, as discussed before by G. Cheng et al. [44]. The circuit can also elevate the possible output energy per cycle, and such effect was discussed in details by Zi et al. [45]. Fig. 5c shows the output current I_{SW} with a resistive load of 100 Ω. The peak of the current can reach 1.77 A, and a single current pulse rises to its maximum at the moment when the switch is closed, then decays exponentially with time. The instantaneous power P_{SW} in such a condition is 313 W, and the instantaneous power density is 414 kW m^{-3}. For the device without a switch circuit, the current is limited by the speed of the mechanical contact-separation motion of two electrodes [42]. While with a switch circuit, the inductive charges transfer as soon as the switch is closed, the process is rather short and is not affected by the speed of the contact-separation motion. This is essentially like the charging or discharging of a capacitor, which has relations of $I_{SW} \propto R^{-1}$ and $P_{SW} \propto R^{-1}$ [44]. Thus the instantaneous current and instantaneous power would drop with increasing resistive load, as shown in Fig. 5d. The results coincide well with previous reports [44]. By using the switch circuit, the device is capable for applications requiring high pulse power.

To test its performance in real water circumstance, the device was put on water surface in a water tank. With the stimulation of water waves [35], the device can work effectively and outputs comparable short-circuit current as that of using the vibration generator, as shown in Fig. 6a. The maximum short-circuit current reaches 174 μA, indicating high working ability on water. To give a direct image of the electricity generated by the device, 600 LEDs are placed on top of the device floating in water (Fig. 6b). These LEDs can be lighted up simultaneously with the electricity generated by the device, as shown in Fig. 6b and Video S1 in Supplementary material. The produced electricity can be further managed and stored in supercapacitors and batteries as a power source for sensors and electronic circuits [25,34].

Supplementary material related to this article can be found online at doi:10.1016/j.nanoen.2016.11.037.

As illustrated above, the device shows superior output performance while possessing merits of light weight, low cost etc. Most importantly, it has excellent extendibility based on the pressure driven mechanism. The number of TENG units in one device can be augmented easily. Thus the output can be greatly enlarged, and potentially meets the requirement to power ocean instruments. The device can also be organized in networks to harvest large-scale water wave energy [35], and transmits the electricity to the land through cables, providing a new route to harvest the renewable and clean ocean energy with low cost.

3. Conclusions

In summary, an integrated triboelectric nanogenerator array device based on air-driven membrane structures is demonstrated. The device shows several superior attributes. First, with a novel design of using air pressure to transfer and distribute harvested water wave energy, the device can drive a series of integrated TENG units effectively and simultaneously. Second, based on the spring-levitated oscillator structure, the dynamics of the device can reach resonance with low frequency water waves, achieving high energy harvesting ability. A device integrating 38 TENG units is presented. While operating at low frequency near the resonant frequency of about 2.9 Hz, the device shows high output of transferred charges per cycle of 15 μC, short-circuit current of 187 μA and optimized peak power density of 13.23 W m^{-3}. Based on the air-driven mechanism, the device can easily integrate large-scale high-density TENG arrays in one package. It can also be organized in large networks. In these ways, the output can be greatly augmented, providing a promising route to effectively harvest water wave energy for various practical applications.

4. Experimental section

4.1. Fabrication of the nanostructures on PTFE surface

PTFE films of 50 μm thick were ultrasonicly cleaned with ethanol and deionized water successively, and dried in a drying oven. A thin layer of Cu film was deposited on the cleaned PTFE surface by sputtering. Then inductively coupled plasma (ICP) etching was carried out to etch the surface. O_2, Ar and CF_4 gases were introduced into the ICP chamber with flow rates of 10.0, 15.0 and 30.0 sccm (standard cubic centimeter per minute) respectively. A power of 400 W was used for plasma generating, and another power of 100 W was used for accelerating plasma ions. The Cu coated PTFE surface was etched for 6 min to obtain the nanostructures.

4.2. Fabrication of the TENG array

First, PTFE films, Cu and Al foils were cut into small pieces with a dimension of 4.5 cm×7.5 cm. Soft membranes, which contained 20% nylon and 80% polyethylene, were cut into a shape that can form an air-pocket-like structure while folded. Then the PTFE films were attached to the Cu foils, which were attached to the soft membranes subsequently. Al foils were attached to the soft membranes in corresponding positions. The PTFE films were treated with an electron injection process to enhance the charge [37]. Finally, the soft membranes were sealed in certain sides to form an array of air-pocket-like structures.

4.3. Fabrication of the TENG device

A separator with a rectangular hole of 12 cm×9 cm in the center was cut from an acrylic board of 4 mm thick. The TENG array was fixed to the hole, and sealed with glue at the four sides. Then the upper and the lower air chamber walls made from soft membrane were fixed on the separator, ensuring air tightness in the two chambers respectively. Then the above entirety was suspended with elastic bands to the outer shell, which was made from acrylic.

4.4. Measurement of the device

The open-circuit voltage was measured by an electrostatic voltmeter (Isoprobe 279). The transferred charges and the current without a switch circuit were measured by an electrometer (Keithley 6514). The pulse current with a switch circuit was measured by a digital oscilloscope (Agilent DSO-X 2014A). The pressure difference was measured by a digital manometer (AZ 82062).

Acknowledgements

Research was supported by the “Thousands Talents” Program for Pioneer Researcher and His Innovation Team, China, the National Key R & D Project from Minister of Science and Technology, China (2016YFA0202704), National Natural Science Foundation of China (Grant No. 51432005, 5151101243, 51561145021, and 61504009), China Postdoctoral Science Foundation (Grant No. 2015M581041) and the Youth Innovation Promotion Association, CAS.

Appendix A. Supplementary material

Supplementary data associated with this article can be found in the online version at doi:10.1016/j.nanoen.2016.11.037.

References

[1] Q. Schiermeier, J. Tollefson, T. Scully, A. Witze, O. Morton, Nature 454 (2008) 816–823.
[2] J. Tollefson, Nature 473 (2011) 134.
[3] M.Z. Jacobson, M.A. Delucchi, G. Bazouin, Z.A.F. Bauer, C.C. Heavey, E. Fisher, S.B. Morris, D.J.Y. Piekutowski, T.A. Vencill, T.W. Yeskoo, Energ. Environ. Sci. 8 (2015) 2093–2117.
[4] D. Gielen, F. Boshell, D. Saygin, Nat. Mater. 15 (2016) 117–120.
[5] S.H. Salter, Nature 249 (1974) 720–724.
[6] J. Tollefson, Nature 508 (2014) 302–304.
[7] E. Callaway, Nature 450 (2007) 156–159.
[8] J. Scruggs, P. Jacob, Science 323 (2009) 1176–1178.
[9] A.F.D. Falcao, Renew. Sust. Energy Rev. 14 (2010) 899–918.
[10] B. Drew, A.R. Plummer, M.N. Sahinkaya, P.I. Mech, Eng. A: J. Pow. 223 (2009) 887–902.
[11] A. Fakharuddin, R. Jose, T.M. Brown, F. Fabregat-Santiago, J. Bisquert, Energy Environ. Sci. 7 (2014) 3952–3981.
[12] S. Razza, S. Castro-Hermosa, A. Di Carlo, T.M. Brown, APL Mater. 4 (2016) 091508.
[13] Z.L. Wang, J.H. Song, Science 312 (2006) 242–246.
[14] G.T. Hwang, Y. Kim, J.H. Lee, S. Oh, C.K. Jeong, D.Y. Park, J. Ryu, H. Kwon, S.G. Lee, B. Joung, D. Kim, K.J. Lee, Energ. Environ. Sci. 8 (2015) 2677–2684.
[15] C.K. Jeong, J. Lee, S. Han, J. Ryu, G.T. Hwang, D.Y. Park, J.H. Park, S.S. Lee, M. Byun, S.H. Ko, K.J. Lee, Adv. Mater. 27 (2015) 2866–2875.
[16] D.R. Patil, Y. Zhou, J.E. Kang, N. Sharpes, D.Y. Jeong, Y.D. Kim, K.H. Kim, S. Priya, J. Ryu, APL Mater. 2 (2014) 046102.
[17] L.D. Zhao, G.J. Tan, S.Q. Hao, J.Q. He, Y.L. Pei, H. Chi, H. Wang, S.K. Gong, H.B. Xu, V.P. Dravid, C. Uher, G.J. Snyder, C. Wolverton, M.G. Kanatzidis, Science 351 (2016) 141–144.
[18] H.Y. Fang, J.H. Bahk, T.L. Feng, Z. Cheng, A.M.S. Mohammed, X.W. Wang, X.L. Ruan, A. Shakouri, Y. Wu, Nano Res. 9 (2016) 117–127.
[19] F.R. Fan, Z.Q. Tian, Z.L. Wang, Nano Energy 1 (2012) 328–334.
[20] Z.L. Wang, Faraday Discuss. 176 (2014) 447–458.
[21] Z.L. Wang, J. Chen, L. Lin, Energy Environ. Sci. 8 (2015) 2250–2282.
[22] G. Zhu, B. Peng, J. Chen, Q.S. Jing, Z.L. Wang, Nano Energy 14 (2015) 126–138.
[23] C. Zhang, W. Tang, C.B. Han, F.R. Fan, Z.L. Wang, Adv. Mater. 26 (2014) 3580–3591.
[24] Y.L. Zi, H.Y. Guo, Z. Wen, M.H. Yeh, C.G. Hu, Z.L. Wang, ACS Nano 10 (2016) 4797–4805.
[25] S.M. Niu, X.F. Wang, F. Yi, Y.S. Zhou, Z.L. Wang, Nat. Commun. 6 (2015) 8975.
[26] S.H. Wang, Y.N. Xie, S.M. Niu, L. Lin, C. Liu, Y.S. Zhou, Z.L. Wang, Adv. Mater. 26 (2014) 6720–6728.
[27] Y.N. Xie, S.H. Wang, S.M. Niu, L. Lin, Q.S. Jing, J. Yang, Z.Y. Wu, Z.L. Wang, Adv. Mater. 26 (2014) 6599–6607.
[28] W. Tang, T. Jiang, F.R. Fan, A.F. Yu, C. Zhang, X. Cao, Z.L. Wang, Adv. Funct. Mater. 25 (2015) 3718–3725.
[29] G. Zhu, Y.S. Zhou, P. Bai, X.S. Meng, Q.S. Jing, J. Chen, Z.L. Wang, Adv. Mater. 26 (2014) 3788–3796.
[30] G. Zhu, J. Chen, T.J. Zhang, Q.S. Jing, Z.L. Wang, Nat. Commun. 5 (2014) 3426.
[31] X. Wen, W. Yang, Q. Jing, Z.L. Wang, ACS Nano 8 (2014) 7405–7412.
[32] Z. Wen, H. Guo, Y. Zi, M.H. Yeh, X. Wang, J. Deng, J. Wang, S. Li, C. Hu, L. Zhu, Z.L. Wang, ACS Nano (2016) 6526–6534.
[33] G. Zhu, Y.J. Su, P. Bai, J. Chen, Q.S. Jing, W.Q. Yang, Z.L. Wang, ACS Nano 8 (2014) 6031–6037.
[34] X.F. Wang, S.M. Niu, Y.J. Yin, F. Yi, Z. You, Z.L. Wang, Adv. Energy Mater. 5 (2015) 1501467.
[35] J. Chen, J. Yang, Z.L. Li, X. Fan, Y.L. Zi, Q.S. Jing, H.Y. Guo, Z. Wen, K.C. Pradel, S.M. Niu, Z.L. Wang, ACS Nano 9 (2015) 3324–3331.
[36] Y. Yang, H.L. Zhang, R.Y. Liu, X.N. Wen, T.C. Hou, Z.L. Wang, Adv. Energy Mater. 3 (2013) 1563–1568.
[37] L.M. Zhang, C.B. Han, T. Jiang, T. Zhou, X.H. Li, C. Zhang, Z.L. Wang, Nano Energy 22 (2016) 87–94.
[38] T. Jiang, L.M. Zhang, X.Y. Chen, C.B. Han, W. Tang, C. Zhang, L. Xu, Z.L. Wang, ACS Nano 9 (2015) 12562–12572.

[39] H. Fang, W.Z. Wu, J.H. Song, Z.L. Wang, J. Phys. Chem. C 113 (2009) 16571–16574.
[40] H.Y. Li, L. Su, S.Y. Kuang, C.F. Pan, G. Zhu, Z.L. Wang, Adv. Funct. Mater. 25 (2015) 5691–5697.
[41] C.K. Jeong, K.M. Baek, S.M. Niu, T.W. Nam, Y.H. Hur, D.Y. Park, G.T. Hwang, M. Byun, Z.L. Wang, Y.S. Jung, K.J. Lee, Nano Lett. 14 (2014) 7031–7038.
[42] S.M. Niu, S.H. Wang, L. Lin, Y. Liu, Y.S. Zhou, Y.F. Hu, Z.L. Wang, Energy Environ. Sci. 6 (2013) 3576–3583.
[43] S.M. Niu, Z.L. Wang, Nano Energy 14 (2015) 161–192.
[44] G. Cheng, Z.H. Lin, L. Lin, Z.L. Du, Z.L. Wang, ACS Nano 7 (2013) 7383–7391.
[45] Y.L. Zi, S.M. Niu, J. Wang, Z. Wen, W. Tang, Z.L. Wang, Nat. Commun. 6 (2015) 8376.

Dr. Liang Xu received his Ph.D. degree from Tsinghua University (THU) in 2012, with awards of Excellent Doctoral Dissertation of THU and Excellent Graduate of Beijing. Before that he achieved bachelor's degree of mechanical engineering in Huazhong University of Science & Technology (HUST) in 2007. He is now a postdoctoral fellow in Beijing Institute of Nanoenergy and Nanosystems, Chinese Academy of Sciences (CAS), under the supervision of Prof. Zhong Lin Wang. His research interests include nanogenerators and self-powered nanosystems, fundamental tribological phenomena, scanning probe microscopy and molecular dynamics simulation.

Yaokun Pang received his undergraduate degree from Qingdao University in 2013, and now he is a doctoral candidate in Beijing Institute of Nanoenergy and Nanosystems, Chinese Academy of Sciences. His research interests are triboelectric nanogenerator, flexible electronic, semiconductors and their applications in self-powered sensor networks and human–machine interaction.

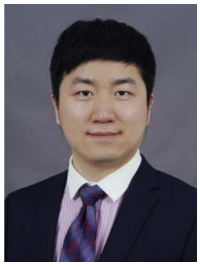

Prof. Chi Zhang received his Ph.D. degree from Tsinghua University in 2009. After graduation, he worked in Tsinghua University as a postdoc research fellow and NSK Ltd., Japan as a visiting scholar. He now is the principal investigator of Tribotronics Group in Beijing Institute of Nanoenergy and Nanosystems, Chinese Academy of Sciences (CAS), Fellow of the NANOSMAT Society, Member of Youth Innovation Promotion Association, CAS, and Youth Working Committee Member of Chinese Society of Micro-Nano Technology. Prof. Chi Zhang's research interests are triboelectric nanogenerator, tribotronics, self-powered MEMS/NEMS, and applications in sensor networks, human-computer interaction and new energy technology. He has been awarded by NSK Sino-Japan Friendship Excellent Paper Award of Mechanical Engineering and granted by National Natural Science Foundation of China, Beijing Natural Science Foundation, China Postdoctoral Science Foundation, and CAS. He has published over 50 papers and attained 13 patents.

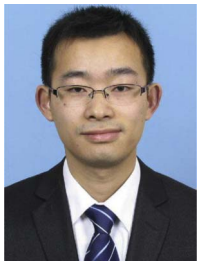

Dr. Tao Jiang received his Ph.D. degree from East China University of Science and Technology in 2014. Now he is an associate researcher in Prof. Zhong Lin (Z.L.) Wang's group at the Beijing Institute of Nanoenergy and Nanosystems, Chinese Academy of Sciences. His research interests are the theoretical studies of triboelectric nanogenerators, and practical applications in self-powered sensing and blue energy harvesting.

Dr. Xiangyu Chen received his B.S. degree in Electrical Engineering from Tsinghua university in 2007 and his Ph.D. in Electronics Physics from Tokyo Institute of Technology in 2013. Now he is an associate professor in Beijing Institute of nanoenergy and nanosystems, Chinese Academic of Sciences. His main research interests have been focused on the field of organic electronics devices, self-powered nano energy system and the nonlinear optical laser system for characterizing the electrical properties of the devices.

Jianjun Luo received his B.S. degree in Chemistry from Jinan University in 2013. He is a Ph.D. candidate in Beijing Institute of Nanoenergy and nanosystems, Chinese Academy of Sciences. His research interests include triboelectric nanogenerators and self-powered nanosystems.

Dr. Wei Tang is an associate professor in Beijing Institute of Nanoenergy and Nanosystems, Chinese Academy of Sciences. He received his B.S. and Ph.D. degree from School of Physics and School of Electronics Engineering and Computer Science, in 2008 and 2013, respectively, from Peking University, China. After graduation, he worked in Beijing Institute of Nanoenergy and Nanosystems as a postdoc research fellow. His research interests include Micro/Nano engineering, triboelectric nanagenerator, self-powered micro/nano system and wireless sensing network.

Prof. Xia Cao is currently a distinguished professor at University of Science and Technology Beijing, and a professor at Beijing Institute of Nanoenergy and Nanosystems, Chinese Academy of Sciences. Her main research interests focus on the energy materials, nanoelectroanalytical chemistry, self-powered nano-biosensors and piezoelectric sensors.

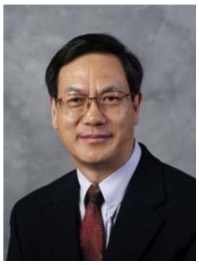

Prof. Zhong Lin Wang received his Ph.D. from Arizona State University in physics. He now is the Hightower Chair in Materials Science and Engineering, Regents' Professor, Engineering Distinguished Professor and Director, Center for Nanostructure Characterization, at Georgia Tech. Prof. Wang has made original and innovative contributions to the synthesis, discovery, characterization and understanding of fundamental physical properties of oxide nanobelts and nanowires, as well as applications of nanowires in energy sciences, electronics, optoelectronics and biological science. His discovery and breakthroughs in developing nanogenerators established the principle and technological roadmap for harvesting mechanical energy from the environment and biological systems for powering a personal electronics. His research on self-powered nanosystems has inspired the worldwide effort in academia and industry for studying energy for micro-nano-systems, which is now a distinct disciplinary in energy research and future sensor networks. He coined and pioneered the field of piezotronics and piezophototronics by introducing piezoelectric potential gated charge transport process in fabricating new electronic and optoelectronic devices. Details can be found at: www.nanoscience.gatech.edu.